SCIENTIFIC REP⦿RTS

Enhanced adaptive focusing through semi-transparent media

Diego Di Battista[1], Giannis Zacharakis[1] & Marco Leonetti[2]

Adaptive optics can focus light through opaque media by compensating the random phase delay acquired while crossing a scattering curtain. The technique is commonly exploited in many fields, including astrophysics, microscopy, biomedicine and biology. A turbid lens has the capability of producing foci with a resolution higher than conventional optics, however it has a fundamental limit: to obtain a sharp focus one has to introduce a strongly scattering medium in the optical path. Indeed a tight focusing needs strong scattering and, as a consequence, high resolution focusing is obtained only for weakly transmitting samples. Here we describe a novel method allowing to obtain highly concentrated optical spots even by introducing a minimum amount of scattering in the beam path with semi-transparent materials. By filtering the pseudo-ballistic components of the transmitted beam we are able to experimentally overcome the limits of the adaptive focus resolution, gathering light on a spot with a diameter which is one third of the original speckle correlation function.

The active control of light propagation through turbid media[1] is becoming an essential tool in microscopy[2], biological and biomedical imaging[3–8], communication technology[9,10], and astrophysics[11,12]. Wavefront shaping[13] is a powerful technique that allows to manipulate the optical paths through scattering media and currently it is possible to generate behind a scattering material multiple light spots, actively driven at user controlled positions[1,14], spatiotemporal focusing[1,15], sub-wavelength foci (which may be employed for high resolution microscopy below the diffraction limit)[16,17], to transmit image around corners[18], to control nonlinear systems[6,19] such as random lasers[20–22] and to permit novel forms of secure communication[23].

These results are achieved by properly adjusting the wavefronts in order to correct for the de-phasing acquired due to the random propagation in the disordered medium. The key enabling technology is the Spatial Light Modulator (SLM), a device which enables a point per point control of the wavefront of a coherent light beam. In practice by setting with the SLM the input beam shape it is possible to control the wavefront at the output of an optical system with an unknown scattering matrix. Various strategies have been developed to obtain light focused at a user defined location: time reversal phase conjugation[24,25], transmission matrix measurement[26,27] or phase scan based algorithms[28–30]. Vellekoop and colleagues demonstrated that the minimum spot size achievable through adaptive focusing in strongly scattering materials is defined by the speckle correlation function[14]: in practice its limit is the speckle grain. The speckle pattern is a random distribution of bright and dark areas due to random interference of countless light paths transmitted through disorder and its grain size depends on the length L and scattering mean free path ℓ[31–33]: in transmission geometry, when the scattering strength increases, the typical grain of the speckle pattern becomes smaller. In order to obtain a tight focus through a scattering sample one has to exploit thick samples because high resolution is obtained in exchange of throughput[34], which is a critical obstacle for modern adaptive super-resolution techniques[16,17], currently limited to low transmittance experiments only. Approaches based on dark field configuration improve visibility at the target[16], but do not allow selecting the speckle components in order to improve the effective resolution of the system. Optical Eigenmode (OEi) approaches were tested to achieve sub-diffraction optical features in free space for minimizing the size of a focused optical field[35]. The combination of particular photonic

[1]Institute of Electronic Structure and Laser, Foundation for Research and Technology-Hellas, N. Plastira 100, Vasilika Vouton, 70013, Heraklion, Crete, Greece. [2]Center for Life Nano Science@Sapienza, Instituto Italiano di Tecnologia, Viale Regina Elena, 291 00161 Rome, Italy. Correspondence and requests for materials should be addressed to D.D.B. (email: dibattista.d@iesl.forth.gr)
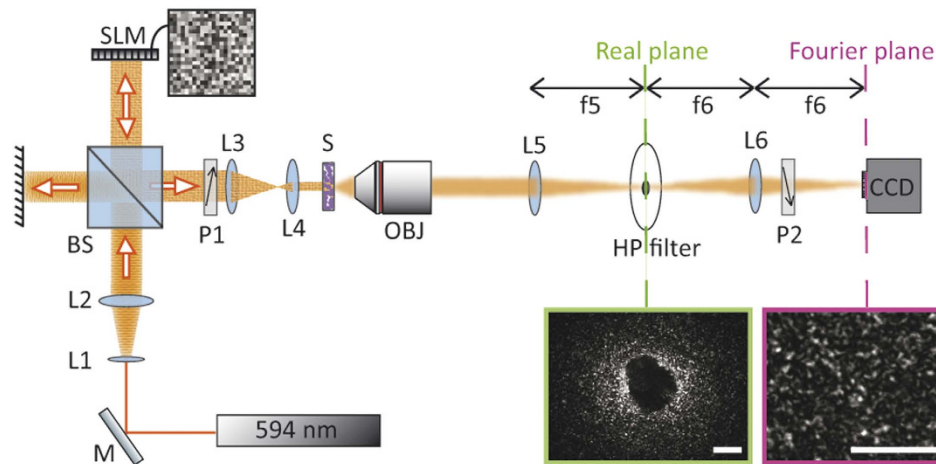
Figure 1. A schematic representation of the experimental setup: a modulated beam from a spatial light modulator is reduced and collimated by a 15X telescope and it impinges onto a scattering layer (S). The transmitted light is used to produce a real image of the sample by lens L5. The image is filtered from its central components by a Spatial High Pass filter (HP filter). The result of the filtering is Fourier transformed onto the camera plane by the lens L6. Polarizers P1 and P2 have perpendicular orientation in order to filter the ballistic contribution. Scale bars correspond to 0.5 mm.

structures and wavefront correction by OEi methods have been exploited to produce subwavelength foci[36,37]. However, to date and to the best of our knowledge, adaptive foci with a resolution under the limit of the speckle pattern correlation function have never been demonstrated.

The current optical techniques adopted for bio-imaging are efficient enough up to the first millimeter in depth (1 transport-mean-free-path)[4] and wavefront modulation appears to be the best solution for correcting imaging quality[3,38] and for suppressing the turbidity[39] at any diffusive regimes. Here we propose an experimental technique which permits to achieve sharp adaptive focusing through weakly scattering samples.

A single speckle pattern results from the superimposed contribution of many different components. Wavefront shaping is an optimization process which aims at maximizing the intensity at the target. In semi-transparent media the larger speckle grains correspond to higher intensities, and hence the focusing process which exploits intensity as a feedback automatically selects configurations with larger grains to increase intensity and thus producing larger foci. In our work, we demonstrate that using the high-pass spatial filter we can select those small grains, which are hidden due to dynamic range limitations, but nevertheless present within the speckle pattern and not accessible otherwise. In other words, by appropriately selecting some of the components during the optimization we exploit hidden degrees-of-freedom that maximize the effective numerical aperture of the opaque lens. Indeed, we can produce a focus smaller than the speckle pattern correlation function, effectively overcoming the theoretical limit previously proposed by Vellekop and coworkers[14] for strongly scattering media. The core idea consists of selecting only those light paths which experienced multiple scattering events by filtering the ones which have experienced only weak scattering. A spatial filter is employed for the selection of the appropriate light paths (modes)[40] and by exploiting a standard phase scan method[30] (see Methods) a stronger focusing with a smaller size speckle pattern is obtained. Furthermore the focus persists also if the filter is removed so that a sharp light spot is obtained within a speckle pattern with a much larger grain. By exploiting our protocol we are able to obtain a focus size approximately 68% smaller than the average speckle grain.

Results

Adaptive focusing with Spatial High Pass filter. The mode filtering relies on custom-made Spatial High Pass filters (HP filter) with diameters ranging from 0.35 mm up to 1.3 mm (see Methods). In Fig. 1a schematic representation of the experimental setup is shown: a SLM modifies the wavefront of the coherent light which impinges onto a scattering sample (S). During propagation through the turbid material, scattering decomposes an incident wave into multiple components which generate a speckle pattern by randomly interfering at the output of the sample. The speckle pattern is collected by an objective lens (OBJ) (see Methods for further details) and is projected behind it. At a distance of 150 mm from the rear face of the OBJ a lens L5 is placed to reproduce the speckle pattern (and a real image of the sample) at its focal length (see Fig. 1). On this plane the HP filter is aligned in order to block the central components of the speckle pattern: these components are related to modes which underwent a few scattering events (hence they are weakly scattered from the ballistic trajectory; we refer to them as "pseudo-ballistic"). Finally a 400 mm lens L6 produces an image on the CCD camera plane which is the conjugate plane
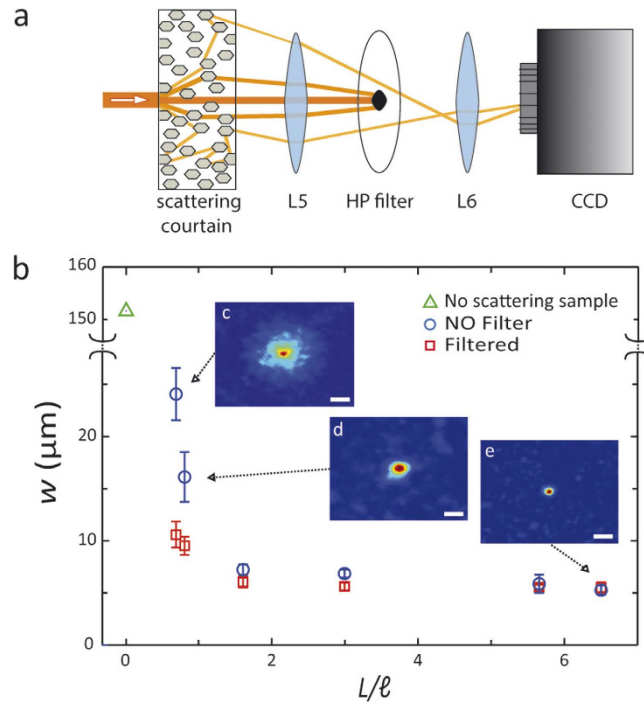
Figure 2. (**a**) Graphical representation of the operating principle of the HP filter: light rays propagating through a weakly scattering medium are focused on the plane of the HP filter. Only light that experiences few scattering events is blocked by the filter, the remaining contributes to the speckle at the camera plane. (**b**) Full Width at Half Maximum of foci obtained at the end of the optimization process plotted as a function of the optical length L/ℓ of the samples. The green triangle represents the beam waist that impinges onto the sample. A comparison between the ordinary approach[14] (no filter, blue circles) and the case with the 0.8 mm diameter HP filter (red squares) is shown. The three insets, starting from the top, correspond to foci obtained at $L/\ell = 0.7$, 0.81 and 6.3. White scale bars correspond to 30 μm.

of the image from L5. The image on the camera is the result of the superposition between modes not blocked by the HP filter or by the Polarizers (P1 and P2 with perpendicular orientations serve to eliminate ballistic contribution). Different samples were illuminated with the same beam waist (0.24 mm) and the back surface of each sample has been aligned on the focal plane of the OBJ. We define the Full Width at Half Maximum, FWHM (w) as the width of the intensity peak around the target spot.

The optimization protocol starts from a random SLM mask, splitting the wavefront into segments with random de-phasing. Then for each one of the segments the phase is shifted (see Methods) and the change is retained if the brightness at the target is enhanced, otherwise the previous configuration is restored. Our experimental setup allows for an *enhancement* factor (η)[13,14] of 250, calculated as the ratio between the intensity at the target and the average intensity of the speckle pattern before optimization. In Fig. 2 we compare the values w obtained with the standard focusing approach[13,14] (without filtering) for different samples characterized by the optical length L/ℓ (blue circles in Fig. 2) with the values obtained when the HP filter is used (red squares in Fig. 2). We study the focusing resolution, measured as the full width at half maximum w for different scattering samples with controlled optical transmittance (sample thickness is varied from a few micrometers to hundreds of micrometers) corresponding to optical lengths between one and ten scattering mean free paths[33] (from $L/\ell = 0.7$ to $L/\ell = 6.5$). The ratio L/ℓ was calculated from the measured direct transmission exploiting a modified Beer-Lambert law[33,41] (see Methods). The results of Fig. 2 obtained for samples with different optical thicknesses L/ℓ, and presented by the blue circles, demonstrate that turbid lenses reach the optimum efficiency for an optical length of the order of the scattering mean free path.

The results of the same experiment with a HP filter applied as presented in Fig. 2 by the red squares, demonstrate that the FWHM of the foci obtained with the filter blocking the pseudo-ballistic modes (see sketch Fig. 2a) is always smaller than the non-filtered case.

A Sharp Adaptive focus in a semi-transparent medium. We characterized the effects of the HP filters demonstrating strong adaptive focusing through semi-transparent materials. We measured the focus width, *w,* as a function of the HP filter diameter *D,* through a semi-transparent sample.
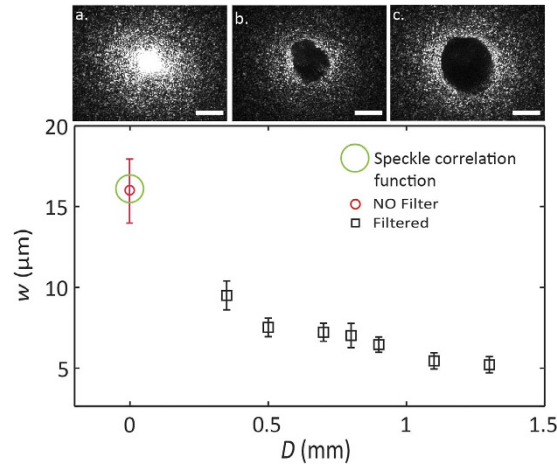
Figure 3. In the upper panel we report the speckle pattern in the plane generated by L5 (see Fig. 1) under three different configurations. Panel (**a**) is the free speckle pattern through a sample with optical length $L/\ell = 0.81$; (**b,c**) are filtered patterns with 0.7 mm and 1.3 mm diameter spatial filter, respectively. Scale bars are equivalent to 0.5 mm. The graph shows the dependence of the focus width w (in black square) versus the HP filter diameter. All data has been collected through a sample with $L/\ell = 0.81$ and is compared to the FWHM of the focus obtained in the absence of a filter (red circle).

Figure 3 reports the results for D varying from 0.35 to 1.3 mm. w decreases by increasing the filter diameter and it is possible to obtain a focus much smaller than the size of the speckle grains. Panel a) on Fig. 3 shows the speckle pattern at the back of the disordered sample (optical length $L/\ell = 0.81$). Panels b) and c) show the same pattern filtered by a 0.7 mm and a 1.3 mm diameter beam stop, respectively. By eliminating the pseudo-ballistic components, our filter selects modes which have suffered stronger scattering and thus produce a larger effective numerical aperture yielding a smaller speckle and a smaller focus. On average (statistics over 10 measurements), we obtained a focus which is of 0.32 ± 0.15 (one third) of that obtained when the filter is absent.

Figure 4a presents a snap-shot of the initial speckle pattern generated through a semi-transparent sample, before the optimization, when the HP filter is not inserted; the pattern composed of large grains with an average diameter of 25 μm estimated from the speckle correlation function. In Fig. 4b we report an image of the focus achieved with a 0.5 mm HP filter. A remarkable effect is observed after the removal of the HP filter; the adaptive focus is not affected and remains smaller than the speckle size as shown in Fig. 4c.

The filtering of the pseudo-ballistic modes is only needed during the optimization procedure, while the sharp focusing is retained after the filter removal. In Fig. 4d we compare the foci profiles. The solid curve correspond to the measurement obtained with the HP spatial filter, while the blue dashed curve corresponds to the standard focusing approach[13,14] without filtering. In this case the effect of the filter is a reduction of the focus size by a factor of 0.52 ± 0.11; moreover, removing the spatial filter does not alter the focus, which maintains the same shape, while being surrounded by larger speckle grains. The focus waist obtained is 12.3 ± 0.8 μm (blue profile in Fig. 4e) which is approximately the same as the size of the focus obtained with the filter (FWHM is of 12.1 ± 0.8 μm, represented by the blue dashed curve in Fig. 4d,e) and is approximately half of the speckle size grains (FWHM of the speckle correlation function is 23.5 ± 2.5 μm, represented by the dotted violet curve in Fig. 4e). When the filter is absent the presence of the pseudo-ballistic modes increases the background signal with respect to the focus intensity decreasing the Peak-to-Background Ratio (η_{PBR}) calculated as the maximum intensity at the target divided by the average intensity of the background. We measured η_{PBR} equal to 196 ± 35 with filter and equal to 16 ± 5 without filter (statistics over 10 measurements). The pseudo ballistic modes (with small numerical aperture) hide the modes associated with strongly scattering light paths (which produce a less intense contribution but a larger effective numerical aperture) making impossible to obtain a sharp focus when both the contributions are interfering on the image plane. This is demonstrated by measurements reported in Fig. 5, where we report the radial distribution of the intensity in the plane of the filter: apparently, when the filter is absent (red curve) the intensity at $\mathbf{r} = 0$ (pseudo ballistic modes) is large. The filter displaces the maximum at larger values of $\mathbf{r}$ thus it selects highly scattering modes.

The ratio of the modulated versus non modulated intensity (I_M/I, see Methods) depends on the filter size D (Fig. 5b red open circles). The black crosses in the same panel show the enhancement η (with filter) as a function of D. In the case studied in Fig. 4, the enhancement drops from $\eta_1 = 196 \pm 35$ (with filter) to $\eta_2 = 16 \pm 5$, a factor $\eta_2/\eta_1 = 0.082$, in perfect agreement with the value of $I_M/I = 0.080$. In a
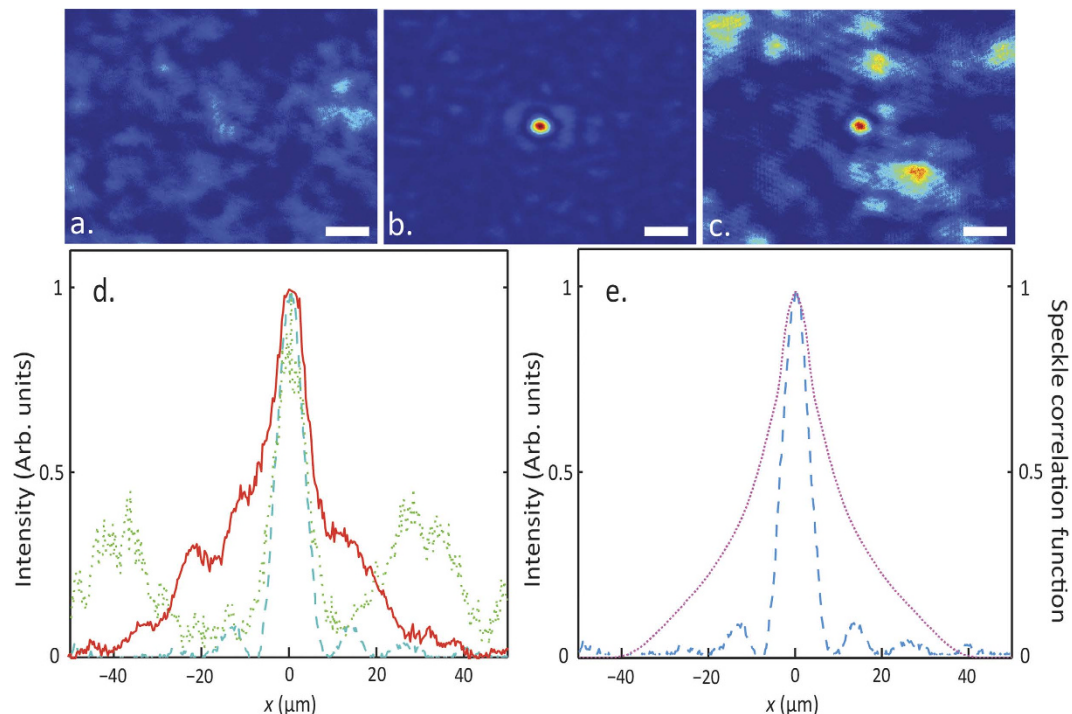
Figure 4. (**a**) speckle pattern obtained through a $L/\ell = 0.7$ scattering sample. (**b**) shows the optimized focus with a 0.5 mm diameter filter for the same sample. (**c**) shows the same as in b but after the filter is removed. Note: the focus still present and smaller than the speckle grain. White scale bars correspond to 30 μm. (**d**) Focusing profiles at the target position without filter (solid red curve), with filter (dashed blue curve) and when the filter is removed (dotted green curve). (**e**) The focus obtained with the filter (dashed blue curve) is compared to the speckle correlation function with a randomly generated wavefront and in the absence of a filter (dotted violet curve).
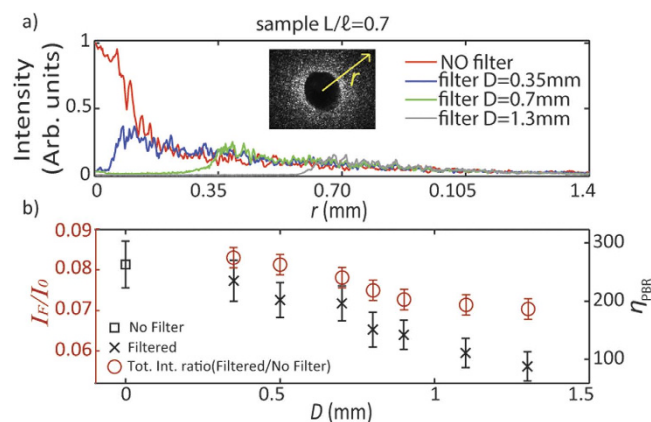
Figure 5. (**a**) the intensity profile along the direction **r** of the speckle pattern in the Real Plane (indicated in Fig. 1) through a $L/\ell = 0.7$ scattering sample. Four different configurations are reported: the red line is the free speckle pattern, blue, green and gray are respectively the profiles with 0.35 mm, 0.7 mm and 1.3 mm diameter spatial filter. (**b**) red circles show the ratio I_M/I as a function of the filter diameter D. The foci enhancements η_{PBR} (black square and black crosses) decrease with the size of the filter since a part of the light controlled by the SLM has been stopped.

nutshell when the filter is removed the signal-to-noise ratio decreases by a factor equal to the amount of non-modulated intensity which is added to the previous speckle.

Discussion

We have demonstrated the enhanced adaptive focusing through weakly scattering media, by the introduction of a spatial filter in the image plane of the produced speckle pattern. The effect is a significant increase of the focusing resolution with a reduction of the spot size below the speckle size defined by the speckle correlation function. The method strongly improves the focusing resolution for turbid samples (turbid lenses) with optical lengths smaller than two scattering mean free path. The introduction of a spatial filter reduces the speckle size because pseudo-ballistic modes possess a reduced span of momentum components (thus producing a smaller effective numerical aperture) with respect to strongly scattered modes. This means that in the weak scattering regime, speckles result from a superposition of patterns possessing different grain size. Our filtering technique, selects a speckle with a smaller size during the optimisation protocol, and this allows the algorithm to exploit degrees of freedom which are "hidden" in the standard focusing optimisation. In fact, in the extremely weak scattering configuration, pseudo-ballistic modes are much more intense than the strongly scattering modes, thus producing a large grained speckle which hides the small grained speckles produced by the strongly scattering channels. With our approach we are thus able to select the components of a speckle pattern producing a focus with the maximum resolution. The presented results not only implement the state-of-art of the adaptive focusing process but may also open the way to a novel generation of high transmission, semi-transparent turbid lenses with high focusing resolution.

Methods

Setup. A coherent laser source emitting at 594 nm is used while a homemade telescope (lens L1 + lens L2) magnifies the laser beam by $10\times$. Modulation is performed by a phase only Spatial Light Modulator (SLM) (Holoeye, Pluto, Berlin-Adlershof, Germany) that shapes the wavefront of the beam; a 50:50 beam splitter (BS) guarantees the beam and the SLM are perpendicular to each other. Hence, 50% of the light reflected by the SLM is directed along a perpendicular axis where a second telescope (lens L3 + lens L4) reduces the beam by $15\times$ to 0.24 mm. A collimated beam impinges onto the scattering sample (S) and the output is collected by a $10\times$ infinity corrected microscope objective (OBJ) with 0.25 numerical aperture. The combination of OBJ, L5 and L6 as described in Fig. 1 creates a magnification on the camera that corresponds to $\times 15$.

Spatial High Pass filter (HP filter) & scattering samples: fabrication and characterization. The HP filters are fabricated by a mixture of 85% black dye used for solvent free resins (Pentasol No 3312, Prochima, Pesaro-Urbino, Italy), 14% Crystal Super Transparent resin (Prochima) and 1% of its catalyst. The liquid mixture is deposited on thin microscope cover slip glasses with a micro-pipette, a process that allowed to control the diameter of the droplet. The mixture is then solidified in an oven at 40ºC for 1 hour. Once the droplet has reached the solid state it remains permanently stable and static. To test the optical properties of the filters we fabricated a 0.40 mm thin film and we measured the absorption (A = 85%), reflection (R = 14.5%) and total transmission (T = 0.5%) with a spectrophotometer (Lambda 950, PerkinElmer, Waltham-Massachusetts, USA). The scattering samples are TiO$_2$ thin layers fabricated by sedimentation of water suspensions and subsequent evaporation of the water. We exploited TiO$_2$ Anatase nano-powder with particle size <25 nm (Sigma-Aldrich, St. Louis, MO,USA). In order to control the optical path-length the concentration of the solution was varied from 2% to 0.5%. Samples were let to sediment and to dry at 30ºC in an oven end we used the evaporation method[42]. In TiO$_2$ slabs absorption can be neglected and elastic scattering is the only loss mechanism. Employing a modified Beer-Lambert Law[32,33,41] we have that after a thickness *L*, a ballistic beam attenuates as:

$$I_{OUT} = I_{IN} \cdot e^{-L/\ell} \tag{1}$$

where I_{OUT} represents the intensity exiting the slab when the intensity I_{IN} impinges on it. Inverting the equation we can estimate the optical length of the sample (L/ℓ), which provides a measure of the scattering properties[41].

Algorithm. A mask is composed on the SLM by 40×40 segments with a 255 grayscale each, corresponding to a fixed de-phasing of the light reflected within a range from 0 up to 5.5π. After setting the target, the algorithm tests a series of 50 random masks picking the one providing the best intensity value at the target position (preliminary optimization). Starting from this configuration, the algorithm starts a routine which tests a phase shift of π and $-\pi$ for a single segment accepting it only if an intensity enhancement on the target is measured, otherwise the previous configuration is restored. This routine is repeated for each segment. The same process is used for testing a phase shift of $\pi/2$ and $-\pi/2$.

I$_M$/I. In order to measure the effective intensity modulated by the SLM during the focusing process when the spatial filter is inserted we grabbed a direct image of the plane of the filter, the total camera counts correspond to the modulated intensity I_M. We compared I_M with the total camera counts from the same plane in absence of filter *I*. The ratio I_M/I evaluates the factor of loss for the Peak-to-Background Ratio enhancement (η_{PBR}) of the focus for the two case without and with the filter.

References

1. Mosk, A. P., Lagendijk, A., Lerosey, G. & Fink, M. Controlling waves in space and time for imaging and focusing in complex media. *Nature photonics* **6,** 283–292 (2012).
2. Maurer, C., Jesacher, A., Bernet, S. & Ritsch-Marte, M. What spatial light modulators can do for optical microscopy. *Laser Photon. Rev.* **5,** 81–101 (2010).
3. Yu, H. *et al.* Recent advances in wavefront shaping techniques for biomedical applications. *Current Applied Physics* **15(5),** 632–641 (2015).
4. Ntziachristos, V. Going deeper than microscopy: the optical imaging frontier in biology. *Nature methods* **7,** 603–614 (2010).
5. Cizmar, T. & Dholakia, K. Exploiting multimode waveguides for pure fibre-based imaging. *Nature communications* **3,** 1027 (2012).
6. Katz, O., Small, E., Guan, Y. & Silberberg, Y. Noninvasive nonlinear focusing and imaging through strongly scattering turbid layers. *Optica* **1,** 170–174 (2014).
7. Liutkus, A. *et al.* Imaging with nature: compressive imaging using a multiply scattering medium. *Scientific reports* **4,** 5552 (2014).
8. Ripoll, J., Yessayan, D., Zacharakis, G. & Ntziachristos, V. Experimental determination of photon propagation in highly absorbing and scattering media. *Journal of the Optical Society of America. A, Optics, image science, and vision* **22,** 546–551 (2005).
9. Carpenter, J., Eggleton, B. J. & Schroder, J. 110 × 110 optical mode transfer matrix inversion. *Optics express* **22,** 96–101 (2014).
10. Shen, X., Kahn, J. M. & Horowitz, M. A. Compensation for multimode fiber dispersion by adaptive optics. *Optics letters* **22,** 2985–2987 (2005).
11. Gruneisen, M., Dymale, R., Rotge, J., DeSandre, L. & Lubin, D. Compensated telescope system with programmable diffractive optics. *Opt. Eng.* **44,** 023201 (2005).
12. Cahoy, K. *et al.* Wavefront control in space with MEMS deformable mirrors for exoplanet direct imaging. *J. Micro/Nanolith.* **13,** 011105–011105 (2013).
13. Vellekoop, I. M. & Mosk, A. P. Focusing coherent light through opaque strongly scattering media. *Optics letters* **32,** 2309–2311 (2007).
14. Vellekoop, I. M., Lagendijk, A. & Mosk, A. P. Exploiting disorder for perfect focusing. *Nature photonics* **4,** 320–322 (2010).
15. Small, E., Katz, O. & Silberberg, Y. Spatiotemporal focusing through a thin scattering layer. *Optics express* **20,** 5189–5195 (2012).
16. van Putten, E. G. *et al.* Scattering lens resolves sub-100 nm structures with visible light. *Physical review letters* **106,** 193905 (2011).
17. Park, J. H. *et al.* Subwavelength light focusing using random Nanoparticles. *Nature photonics* **7,** 454–458 (2013).
18. Katz, O., Small, E. & Silberberg, Y. Looking around corners and through thin turbid layers in real time with scattered incoherent light. *Nature photonics* **6,** 549–553 (2012).
19. Katz, O., Small, E., Bromberg, Y. & Silberberg, Y. Focusing and compression of ultrashort pulses through scattering media. *Nature photonics* **5,** 372–377 (2011).
20. Leonetti, M., Conti, C. & Lopez, C. Switching and amplification in disordered lasing resonators. *Nature communications* **4,** 1740 (2013).
21. Bachelard, N., Andreasen, J., Gigan, S. & Sebbah, P. Taming random lasers through active spatial control of the pump. *Physical review letters* **109,** 033903 (2012).
22. Zacharakis, G., Papadogiannis, N. A., Filippidis, G. & Papazoglou, T. G. Photon statistics of laserlike emission from polymeric scattering gain media. *Optics letters* **25,** 923–925 (2000).
23. Goorden, S. A., Horstmann, M., Mosk, A. P., Škorić, B. & Pinkse, P. W. H. Quantum-secure authentication of a physical unclonable key, *Optica* **1(6),** 421–424 (2014).
24. Yaqoob, Z., Psaltis, D., Feld, M. S. & Yang, C. Optical Phase Conjugation for Turbidity Suppression in Biological Samples. *Nature photonics* **2,** 110–115 (2008).
25. Cui, M. & Yang, C. Implementation of a digital optical phase conjugation system and its application to study the robustness of turbidity suppression by phase conjugation. *Optics express* **18,** 3444–3455 (2010).
26. Yoon, J., Lee, K. R., Park, J. & Park, Y. K. Measuring optical transmission matrices by wavefrontshaping. *arXiv* preprint:1502.04761, (2015).
27. Popoff, S. M. *et al.* Measuring the transmission matrix in optics: an approach to the study and control of light propagation in disordered media. *Physical review letters* **104,** 100601 (2010).
28. Yilmaz, H., Vos, W. L. & Mosk, A. P. Optimal control of light propagation through multiple-scattering media in the presence of noise. *Biomedical optics express* **4,** 1759–1768 (2013).
29. Conkey, D. B., Brown, A. N., Caravaca-Aguirre, A. M. & Piestun, R. Genetic algorithm optimization for focusing through turbid media in noisy environments. *Optics express* **20,** 4840–4849 (2012).
30. Vellekoop, I. M. & Mosk, A. P. Phase control algorithms for focusing light through turbid media. *Optics communications* **281,** 3071–3080 (2008).
31. de Boer, J. F., van Albada, M. P. & Lagendijk, A. Transmission and intensity correlations in wave propagation through random media. *Physical review. B, Condensed matter* **45,** 658–666 (1992).
32. Kop, H. J., de Vries, P. M., Sprik, R. & Lagendijk, A. Observation of Anomalous Transport of Strongly Multiple Scattered Light in Thin Disordered Slabs. *Physical review letters* **79,** 4369–4372 (1997).
33. Garcia, P. D., Sapienza, R. & Lopez, C. Photonic glasses: a step beyond white paint. *Adv Mater* **22,** 12–19 (2010).
34. Davy, M., Shi, Z. & Genack, A. Z. Focusing through random media: Eigenchannel participation number and intensity correlation. *Phys. Rev. B* **85,** 035105 (2012).
35. Baumgartl, J. *et al.* Far field subwavelenght focusing using optical eigenmodes through random media: Eigenchannel participation number and intensity correlation. *Appl. Phys. Lett.* **98,** 181109 (2011).
36. Mazilu, M., Baumgartl, J., Kosmeier, S. & Dholakia, K. Optical Eigenmodes; exploiting the quadratic nature of the energy flux and of scattering interactions. *Optics Express* **19,** 933–945 (2011).
37. De Tommasi, E. *et al.* Biologically enabled sub-diffractive focusing. *Optics Express* **22,** 27214–27227 (2011).
38. Dene Ringuette, *et al.* Reducing misfocus-related motion artefacts in laser speckle contrast imaging, *Biomedical Optics Express* **6,** Issue 1, 266–276 (2015).
39. McDowell, E. J., Cui, M., Vellekoop, I. M., Senekerimyan, V., Yaqoob, Z. & Yang, C. Turbidity suppression from the ballistic to the diffusive regime in biological tissues using optical phase conjugation. *Journal of biomedical optics* **15(2),** 025004–025004 (2010).
40. Goodman, J. W. *Introduction to Fourier Optics.* McGraw-Hill Companies, Inc., New York, (1996).
41. García, P. D., Sapienza, R., Toninelli, C., López, C. & Wiersma, D. S. Photonic crystals with controlled disorder. *Physical Review A* **84,** 023813 (2011).
42. García, P. D., Sapienza, R. & López, C. Photonic glasses: A step beyond white paint. *Adv. Mater,* **22,** 12–19 (2010).

Acknowledgements

Author Contributions

All authors have contributed to the development and/or implementation of the concept. D.D.B. and M.L. ideated and designed the experiment. D.D.B. realized the experimental apparatus and performed the measurements. G.Z. analyzed the data and supported the development of the experiment.

Additional Information